UNIVERSITY OF CALIFORNIA SAN DIEGO

Holistic Design Consideration of Metal-Organic Framework-Based Membranes for Lithium-Sulfur Batteries

A Thesis submitted in partial satisfaction of the requirements
for the degree Master of Science

in

NanoEngineering

by

Dong Ju Lee

Committee in charge:

Professor Zheng Chen, Chair
Professor Ping Liu
Professor Tod Pascal

2022

The Thesis of Dong Ju Lee is approved, and it is acceptable in quality and form for publication on microfilm and electronically.

University of California San Diego

2022

TABLE OF CONTENTS

LIST OF FIGURES

LIST OF TABLES

ACKNOWLEDGEMENTS

First, I would like to express my sincere appreciation to my advisor, Prof. Zheng Chen. His guidance, support, and encouragement has enabled me to not only finish this work, but also learn how to think critically as a researcher. I also thank my mentor, Dr. Guorui Cai. His passion has sparked my passion in research, and his patience has helped me to develop mindsets and skillsets necessary as a researcher.

Second, I would like to thank Prof. Seth M. Cohen for his insightful comments on this work. I would like to thank I would also like to thank my committee members, Prof. Ping Liu and Prof. Tod Pascal for their valuable time and comments.

Finally, I would like to thank lab mates, Xiaolu Yu, Dr. Mingqian Li, and Dr. R. Eric Sikma, who have supported me with material synthesis and characterizations for this work.

This work was supported by the National Science Foundation through the U.C. San Diego Materials Research Science and Engineering Center (UCSD MRSEC). This work was performed in part at the San Diego Nanotechnology Infrastructure (SDNI) of U.C. San Diego. Material characterization was supported by a grant from the Department of Energy, Office of Basic Energy Sciences, Division of Materials Science and Engineering.

This work is currently being prepared for submission for publication: Dong Ju Lee, Xiaolu Yu, R. Eric Sikma, Mingqian Li, Seth M. Cohen, Guorui Cai*, and Zheng Chen*, “Holistic Design Consideration of Metal-Organic Framework-Based Membranes for Lithium-Sulfur Batteries”. The thesis author was the primary author of this publication.

ABSTRACT OF THE THESIS

Holistic Design Consideration of Metal-Organic Framework-Based Membranes for Lithium-Sulfur Batteries

by

Dong Ju Lee

Master of Science in NanoEngineering

University of California San Diego, 2022

Professor Zheng Chen, Chair

Metal-organic framework (MOF)-based membranes have received significant attention as separators for lithium-sulfur (Li-S) batteries due to their high porosities, well-defined and tailored structures, and other tunable features that are desirable for preventing the 'shuttle effect' of soluble polysulfides. Due to the insulating properties of most MOFs, composite membranes generally consist of a combination of MOFs and electrically conductive materials. In this study, we examined the property-performance relation between MOF-based separators by systematically adjusting the electrical conductivity, thickness and mass loading of MOF-based separators. Beyond the commonly referenced trapping or blocking ability of MOFs toward polysulfides, we

find that by fixing the thickness of the MOF-based composite coating layer (~ 40 μm) on a Celgard membrane, the electrical conductivity of the MOF composite layer is of paramount importance to the cycling performance compared with the physical/chemical trapping ability of polysulfides. However, the trapping ability of MOFs becomes essential when the thickness of the composite layer is small (*e.g.*, ~ 20 μm), indicating the synergetic effects of the adsorption and conversion capabilities of the thin composite layer. This work suggests the importance of a holistic design consideration for MOF-based membrane for long-life and high energy density Li-S batteries.

CHAPTER 1. INTRODUCTION

1.1 Lithium-sulfur batteries and the shuttle effect

Lithium-sulfur (Li-S) batteries have been considered as potential next-generation energy storage devices due to their high energy density (2600 Wh kg^{-1}), as well as the natural abundance and low environmental footprint of sulfur.[1-4] However, the practical application of Li-S batteries is impeded by the 'shuttle effect' caused by the migration of soluble reaction intermediates, lithium polysulfide (LiPS, Li_2S_n, $4 \leq n \leq 8$) species, which dissolve in the electrolyte and diffuse across the separator to the lithium anode. The diffused LiPS species then undergo a parasitic reaction and deposit Li_2S/Li_2S_2 on the lithium anode surface, leading to the loss of active material, corrosion of lithium anode, consumption of electrolyte and decreased Coulombic efficiency (Figure 1).[5-9] To address these issues, studies have been focused on modifying the commercial separators with nanoporous materials to block or trap the diffusion of LiPS species.[9-14] Among many candidate materials that have been studied are carbon-based materials, metal oxides, and metal-organic frameworks (MOFs), the latter of which have been widely investigated due to their high porosities and well-defined, tunable pore sizes.[15-20]

Figure 1. A scheme of Li-S batteries illustrating working mechanism and the shuttle effect. Figure reproduced from Reference 4.

1.2 MOF-based membranes for Li-S batteries

Initial approach of preventing the capacity loss was to block LiPS migration to the anode (Figure 2). Despite the improved cycling performance of Li-S batteries by using MOF modified separators,[21-23] the trapped LiPS species within the MOF pores are difficult to re-utilize for subsequent cycling due to the insulating nature of most MOFs, thereby leading to a irreversible loss of the cycling capacity.[24, 25] To overcome this issue, researchers have mixed MOFs with conductive materials to provide electron pathways, so that the trapped LiPS species in the separator can be more effectively re-utilized during the repeating charging/discharging process.[26-30] Although many of the previous studies attribute the improved performance to the physical/chemical blocking and trapping effect of MOFs toward LiPS species,[27, 30, 31] the underlying mechanism of how each component and their interplay in the composite influences the battery performance is still unclear.

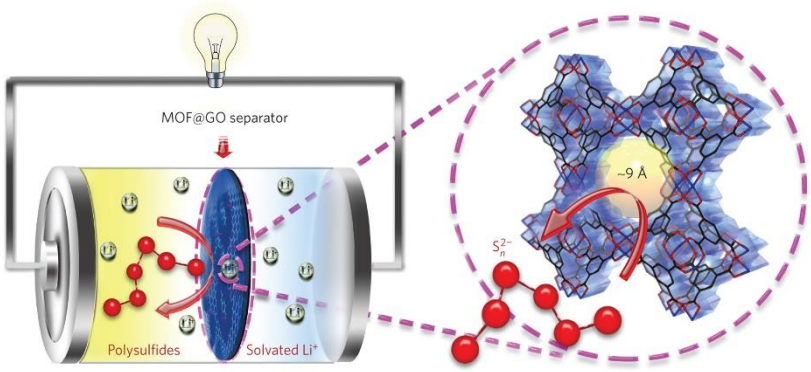

Figure 2. A scheme of MOF-based membranes to block LiPS by using narrow pores of MOFs. Figure reproduced from Reference 23.

1.3 Thesis organization

In this work, we reconsider the property-performance relation between MOF-based composite separators and Li-S batteries by systematically adjusting the electrical conductivity of the MOF-based composite coating layer. UiO-66-NH_2 (UiO = University of Oslo), a Zr(IV)-based

MOF, was adopted as a model material to design and fabricate MOF-based composite separators with tunable electrical conductivity. UiO-66-NH_2 powder was mixed with Super P (SP) carbon black and polymer binder at different ratios and cast on a commercial Celgard 2500 membrane with controlled thicknesses (~40 μm) of the coating layer. Using the composite layer (MOF/SP) modified Celgard as the separator, Li-S half cells were assembled for long-term cycling and rate capability tests, which showed that the cycling performance was strongly correlated with the electrical conductivity of the MOF/SP layer. The composite coating layers with higher SP content show improved initial capacity, capacity retention, and lower overpotential, which is primarily due to the increased sulfur utilization and reduced impedance attributed to the increased electron network available for the conversion reaction. However, when the thickness of the coating layer is small (*e.g.*, ~20 μm), the adsorption property of the MOF plays a more critical role in improving the battery performance. This study shows that the Li-S battery performance is highly dependent on the mass loading and thickness of the MOF-based composite membrane, as well as the ratio of each component. An optimal balance between the adsorption and conversion capabilities of the MOF-based composite layer is of great importance to reduce the mass loading and thickness of inactive layers for high energy density of batteries. This work suggests the importance of a holistic design consideration for MOF-based membrane for long-life and high energy density Li-S batteries.

CHAPTER 2. EXPERIMENTAL SECTION: MATERIALS AND ELECTROCHEMICAL CHARACTERIZATIONS

2.1 Preparation of UiO-66-NH_2

Synthesis of UiO-66-NH_2 was performed according to the documented method with some modifications.[32] Typically, $ZrCl_4$ (612 mg) and 2-aminoterephthalic acid (NH_2-H_2bdc) (466 mg) were dissolved in *N*,*N*-dimethylformamide (DMF) (150 mL) in a Teflon-lined reaction bottle, and the solution was sonicated for 30 min. Acetic acid (29.5 mL) and H_2O (125 μL) were added into the solution, and the mixture was heated at 120 °C for 24 h. After cooling to room temperature, the powder was collected by a centrifugation, washed with DMF and ethanol, and dried under vacuum at 120 °C for 24 h (Figure 3).

Figure 3. An optical image of UiO-66-NH_2 powder after drying.

2.2 Preparation of MOF/SP coated separators

MOFs and SP carbon black with desired weight ratio were manually ground for at least 15 min until the mixture showed a uniform color. The combined MOF/SP powder were mixed with polyvinylidene fluoride (PVDF) to a weight ratio of 90:10 in *N*-methyl-2-pyrrolidone (NMP) by a Thinky mixer. Subsequently, additional NMP solvent was added depending on the different ratios

to produce a viscous slurry. The resulting slurry was cast on a Celgard 2500 separator by a doctor blade to control the coating thickness. After drying under vacuum at 80 °C for 24 h, the coated separator was cut into a disk with a diameter of 18 mm for cell assembly or a rectangle shape of 10×25 mm for electrical conductivity measurement. The MOF/SP coated separators were dried under vacuum at 80 °C overnight before usage.

2.3 Preparation of sulfur cathodes

Sulfur and Ketjen Black were ground with a weight ratio of 8:2 and heated at 155 °C for 12 h in a stainless-steel autoclave. After cooling, the mixture was ground again and heated at 170 °C for 12 h. The prepared sulfur/Ketjen Black, SP, and PVDF with a weight ratio of 70:15:15 were mixed and dispersed in NMP by a Thinky mixer. For making sulfur composite cathode with MOFs, MOFs, sulfur/Ketjen Black, SP, and PVDF were mixed with a weight ratio of 15:70:15:15. The slurry was cast on carbon-coated aluminum foil by a doctor blade and then dried under vacuum at 70 °C for 4 h and overnight with heating turned off. The electrode was cut into a disk with a diameter of 12 mm.

2.4 Lithium polysulfide adsorption test

The Li_2S_6 solution was prepared by dissolving Li_2S and sulfur with a molar ratio of 1:5 in 1,3-dioxolane (DOL) and 1,2-dimethoxyethane (DME) (1:1 by volume), with stirring and heating at 70 °C for 3 days. 15 mg of MOFs or SP powders were soaked in 1.5 mL of the corresponding Li_2S_6 solution in an Ar-filled glovebox, and the solutions were sealed with Teflon-lined caps and transferred out for the adsorption test.

2.5 Electrochemical testing

All electrochemical data were collected using CR-2032 type coin cells assembled in Ar-filled glovebox. 60 μL of 1 M lithium bis(trifluoromethane sulfonimide) (LiTFSI) with 0.2 M $LiNO_3$ in DOL/DME (1/1 by volume) electrolyte (1 M LiTFSI 0.2 M $LiNO_3$ DOL/DME) was used for all cells. The galvanostatic tests were conducted on Neware cyclers, where Li-S half cells were activated at 0.1 A g^{-1} for 3 cycles with the fixed voltage range at 1.8 to 2.8 V before the long-term cycling or rate capability test. Cyclic voltammetry (CV) and electrochemical impedance spectroscopy (EIS) measurements were conducted on Autolab electrochemical workstation. The scan rate and voltage range were 0.1 mV s^{-1} and 1.8 to 2.8 V with one activation cycle for the CV measurement, and the frequency range and amplitude were 1 MHz to 0.1 Hz and 0.01 V for EIS, respectively.

2.6 Material characterization

N_2 sorption isotherms of MOFs were collected on a Micromeritics ASAP 2020 Adsorption Analyzer at 77 K. Powder X-ray diffraction (PXRD) patterns of MOFs were obtained on a Bruker D8 Advance diffractometer using Cu Kα radiation. Morphologies of the MOF/SP modified separators were obtained on a FEI Quanta 250 and Apreo scanning electron microscope (SEM). The in-plane electrical conductivity of the MOF/SP coating layer was measured by a four-probe method with a Keithley 2400.

CHAPTER 3. ELECTROCHEMICAL TESTING AND ANALYSIS

3.1 LiPS adsorption property and trapping effect of MOFs

Considering its high porosity, electrochemical stability and polar functional group (Figure 4), UiO-66-NH_2 was selected as a model MOF material to study its trapping effect on cell stability.[32] To evaluate the interaction between MOFs and LiPS species, a LiPS adsorption test was conducted by soaking an equal weight of UiO-66-NH_2 or SP powders into 1 mM Li_2S_6 in DOL/DME (1/1 by volume) (Figure 5). After 6 h, the UiO-66-NH_2-soaked solution became nearly

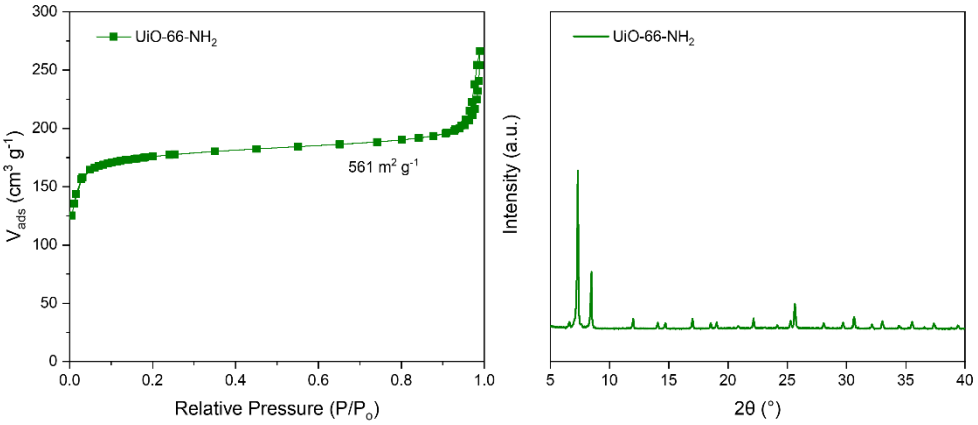

Figure 4. N_2 sorption isotherms and Powder XRD pattern of UiO-66-NH_2.

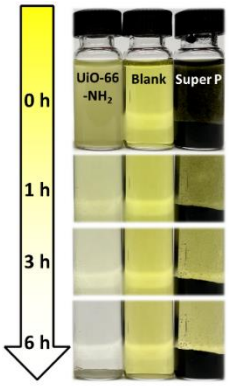

Figure 5. Optical photographs showing LiPS adsorption test of UiO-66-NH_2 and SP in 1 mM Li_2S_6 DOL/DME (1/1 by volume).

transparent, which can be attributed to the adsorption of Li_2S_6 into MOF pores, driven by the trapping effect of nanopores and its interaction with the polar functional groups ($-NH_2$).[33-35] By contrast, the SP-soaked solution showed no noticeable difference compared to the blank solution (1 mM Li_2S_6 in DOL/DME), indicating a weak adsorption ability of SP toward LiPS species.

To better understand how the LiPS adsorption property of MOFs influences the performance of Li-S batteries, MOFs were installed in two different locations inside a coin cell: (i) inside sulfur cathode and (ii) on Celgard separator (Figure 6a). By placing MOFs on the Celgard separator, MOFs can be expected to effectively adsorb or trap LiPS species that diffuse across the separator. On the other hand, by adding MOFs inside the sulfur cathode, the MOFs can be expected

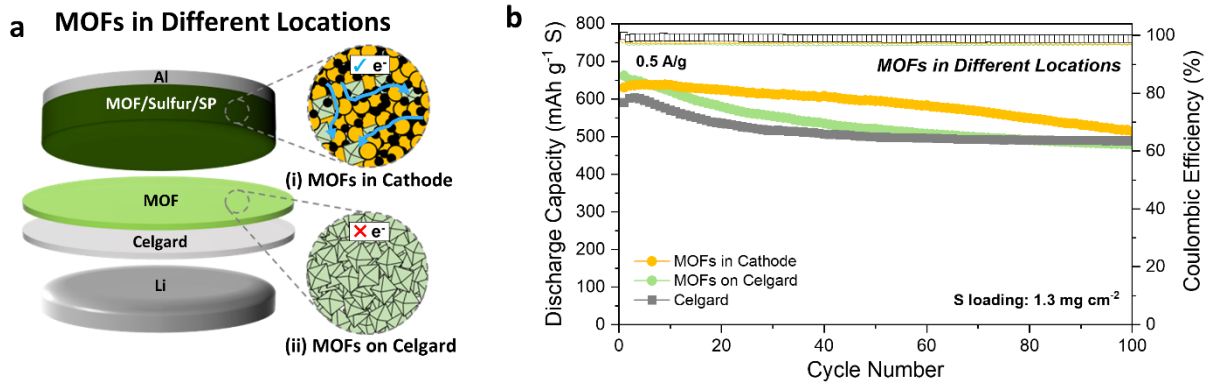

Figure 6. (a) Schematic showing two types of coin cell configuration by placing MOFs in different locations: (i) MOFs in sulfur cathode and (ii) MOFs on Celgard separator. (b) Cycling performance of Li-S half cells with MOFs in different locations in the cell.

to adsorb LiPS formed during redox reaction and re-utilize LiPS by taking advantage of the electrically conductive nature of cathode formed by SP. Li-S half cells were assembled and cycled at 0.5 A g^{-1} with 1 M LiTFSI 0.2 M $LiNO_3$ DOL/DME (Figure 6b). The cell with MOFs on Celgard gives a slightly higher capacity for the first 80 cycles compared to pristine Celgard, but capacity starts to fade even lower than the pristine Celgard after 80 cycles. However, the cell with MOFs

in the sulfur cathode gives better capacity retention and higher capacities than both pristine Celgard or MOF-coated Celgard for more than 100 cycles. The different trend in capacity decay by placing MOFs in different locations of the cell implies that introducing MOFs into electron pathways could be more important than solely blocking the migration of LiPS to the anode side.

3.2 Effect of electrical conductivity of MOF/SP separator

To further understand the importance of the electron pathway connected to MOF particles, we systematically adjusted the electrical conductivity of MOF-based separators by changing the ratio between MOFs and SP in the coating layer (Figure 7a). The SP was chosen as the conductive material in the coating layer because it was also used as conductive additive in the cathode. The

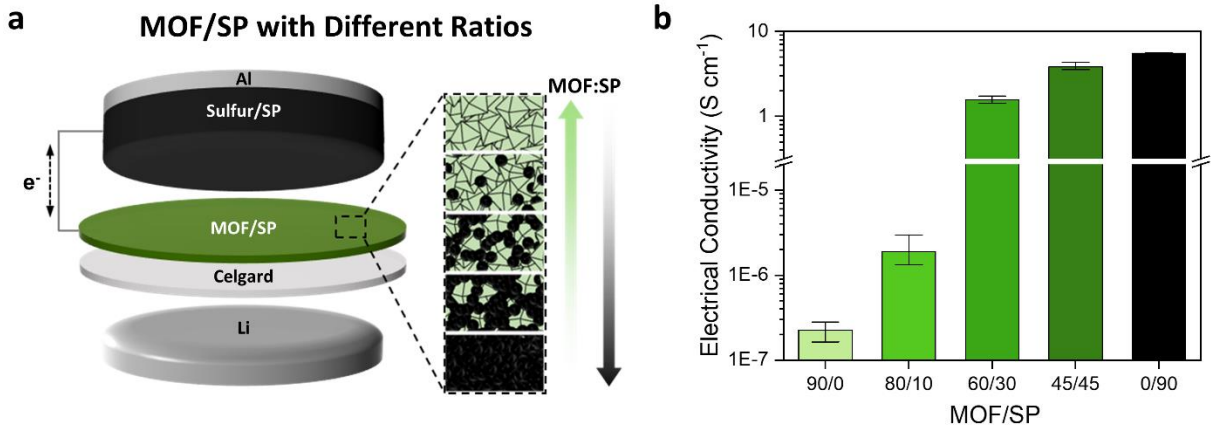

Figure 7. (a) A scheme and (b) electrical conductivity of MOF/SP modified separator with different ratios.

top and cross-sectional scanning electron microscopy (SEM) images (Figure 8) show a uniform mixture of MOFs and SP in the coating layer and similar coating thicknesses (~40 μm) of composite layers with different MOF to SP ratios. Optical and SEM images of the backside of MOF/SP modified Celgard membranes show no penetration of MOFs or SP particles through the

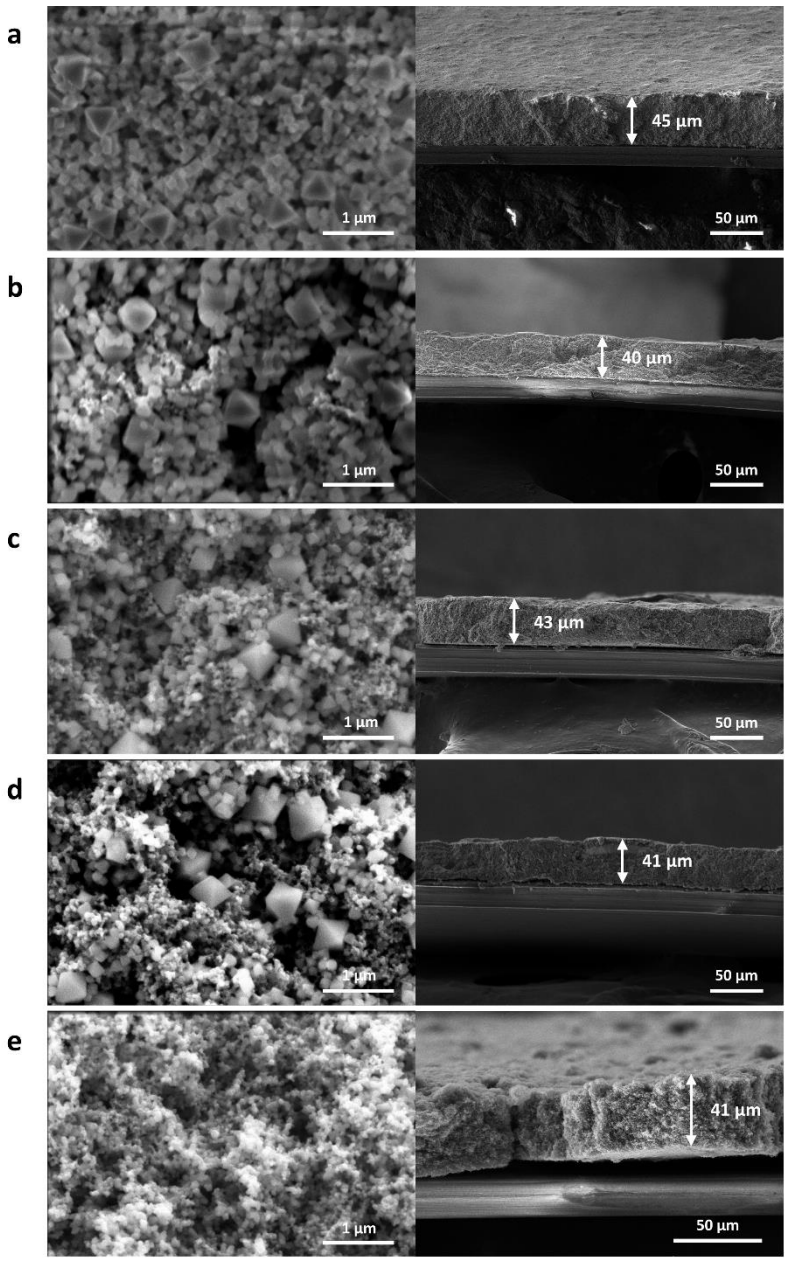

Figure 8. Top and cross-sectional SEM images of the modified Celgard membranes with MOF/SP ratios of (denoted as a MOF/SP ratio based on wt% MOF, wt% SP, and 10 wt% PVDF): (a) 90/0, (b) 80/10, (c) 60/30, (d) 45/45 and (e) 0/90.

membrane (Figure 9), indicating that the insulating function of the separator is maintained after modifying one side with conductive material. Table 1 shows the thickness and mass loading data of modified separators used in this work as well as a description of the experimental design. As expected, the trend in electrical conductivity of the MOF/SP layer followed the increased SP

content in the layer, where higher SP content gave higher electrical conductivity for the MOF/SP composite (Figure 7b). The pure MOF-coated layer (denoted as MOF/SP 90/0 based on 90 wt% MOF, 0 wt% SP, and 10 wt% PVDF) showed electrical conductivity of 2.3×10^{-7} S cm^{-1} with a slightly higher value of 1.9×10^{-6} S cm^{-1} obtained for MOF/SP 80/10. The pure SP coated layer (MOF/SP 0/90) shows a high electrical conductivity of 5.5 S cm^{-1}, and the equal mass mixture (MOF/SP 45/45) gave a comparable electrical conductivity (3.8 S cm^{-1}).

Table 1. A summary of thickness and mass loading of MOF/SP composite layers and description of experimental design.

Composite Layer	Thickness (μm)	Mass loading (mg cm^{-2})	MOF loading (mg cm^{-2})	Figures	Description
MOF/SP 0/90	41	1.4	0	6-17	Fixed thickness with sufficient diffusion length but different MOF/SP ratios to evaluate electrical conductivity effect
MOF/SP 45/45	43	2.7	1.2		
MOF/SP 80/10	40	2.8	2.2		
MOF/SP 90/0	45	3.3	3.0		
MOF/SP 0/90	24	0.9	0	18, 19	Reduced thickness without MOFs to evaluate conversion and adsorption capabilities
	17	0.6	0		
MOF/SP 45/45	25	2.0	0.90	18, 19	Reduced thickness with MOFs to evaluate conversion and adsorption capabilities
	18	1.3	0.59		
MOF/SP 45/45	18	1.3	0.59	20	Fixed MOF/SP ratio but reduced composite loading to evaluate performance limit
	-	0.6	0.27		
	-	0.2	0.09		
MOF/SP 0/90	-	0.6	0	21	Fixed composite loading but reduced MOF/SP ratio to evaluate a balance between conversion and adsorption capabilities
MOF/SP 10/80	-	0.6	0.06		
MOF/SP 30/60	-	0.6	0.18		
MOF/SP 45/45	-	0.6	0.27		

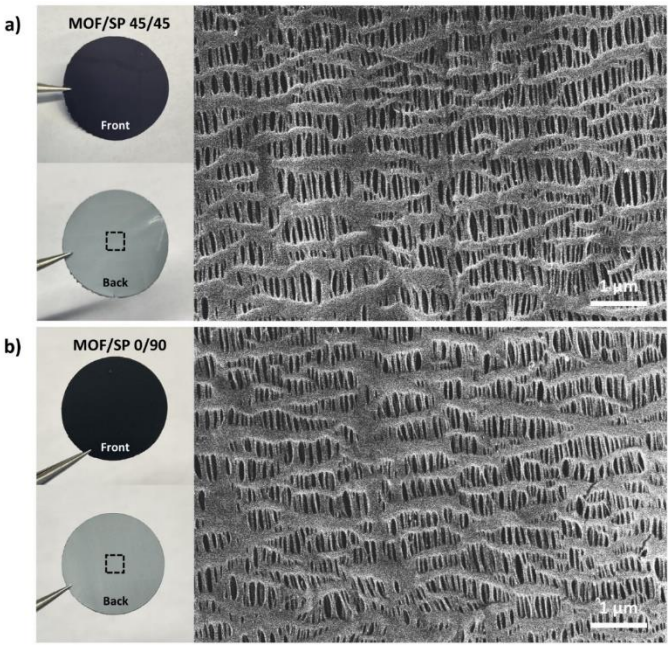

Figure 9. Optical images of front and back surfaces (left) and SEM images (right) of the backside of: (a) MOF/SP 45/45 and (b) MOF/SP 0/90.

To demonstrate how different electrical conductivity influences the performance of Li-S batteries, half cells were assembled with sulfur cathodes (1.3 mg cm^{-2}) and 1 M LiTFSI 0.2 M $LiNO_3$ DOL/DME electrolyte by using the MOF/SP modified Celgrard membrane as the separator and a pristine Celgard membrane as the control. The initial capacities at 0.5 A g^{-1} (Figure 10a) are 590, 662, 714, 975, and 1084 mAh g^{-1} (based on S mass) for the cells with Celgard, MOF/SP 90/0, 80/10, 45/45, and 0/90, respectively. The increased initial capacity with the increased SP content

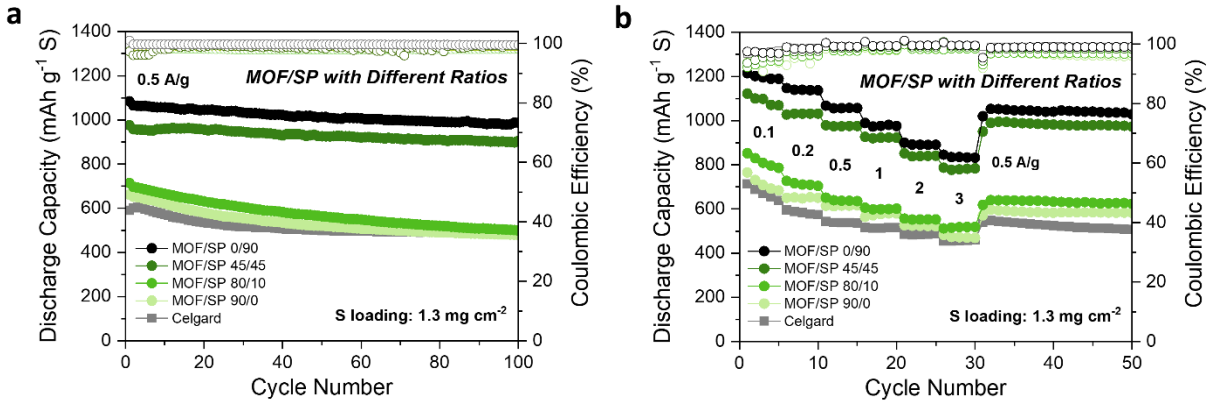

Figure 10. (a) Cycling performance and (b) rate capability of MOF/SP modified separators.

in the coating layer can be explained by the increased sulfur utilization from the conductive carbon.[36] Due to the intimate contact between the cathode and MOF/SP coating layer, the electrically conductive layer can promote efficient utilization of sulfur. Moreover, the improved performance with more SP content indicates that the coating layer can work as a secondary current collector, in which LiPS diffuse into the coating layer and are re-utilized in the redox reaction. Because the electrical conductivity of the secondary current collector determines how effective LiPS can be utilized, the initial capacity and capacity retention hugely depend on the electrical conductivity of the coating layer. In addition, the rate capability was conducted (Figure 10b). At all rates, the modified separators with more SP content gave higher capacity and Coulombic efficiency, highlighting the importance of electrical conductivity of the coating layer at different rates.

Furthermore, in order to decouple the effect of electrical conductivity and the adsorption capability, another layer of Celgard membrane was placed between the cathode and MOF/SP composite layer (Figure 11a). Both the capacities of Li-S cells with MOF/SP 45/45 and 0/90 significantly decreased after electrically isolating the composite layer (Figure 10a and 11b),

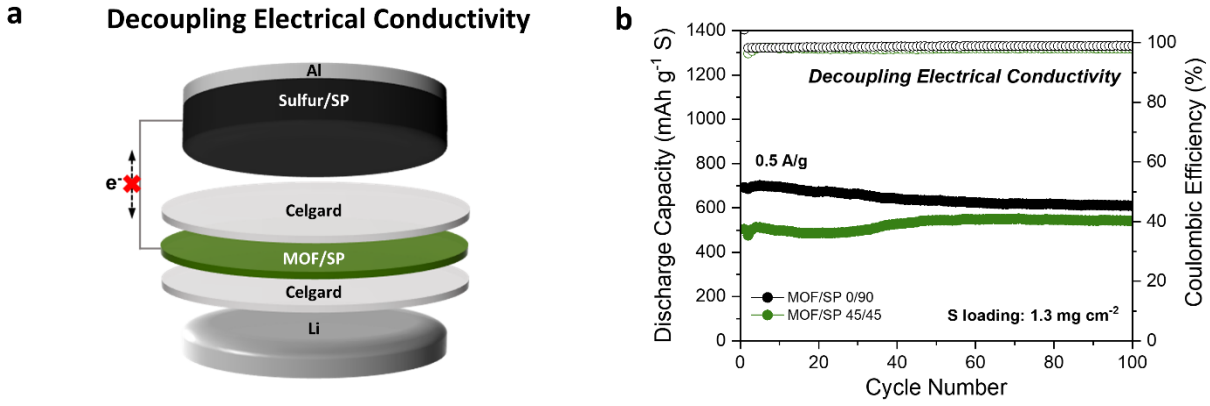

Figure 11. (a) A scheme and (b) cycling performance of electrically insulated MOF/SP modified separator by adding one layer of Celgard membrane between cathode and MOF/SP layer.

confirming that the performance enhancement of the MOF-based composite is mainly a result of electrical conduction. In addition, the lower capacities of MOF 45/45 compared to 0/90 can be attributed to the continuous LiPS adsorption by MOF particles that form isolated (inactive) LiPS. These results clearly show that electrical conductivity of the composite layer is strongly correlated with the Li-S battery performance.

3.3 Electrochemical analysis of MOF/SP separator

To better understand the electrochemical properties of the MOF/SP modified separators, voltage profiles, CV, and EIS were analyzed. The voltage profiles at different charge/discharge rates show the increase of overpotential with the decrease of electrical conductivity of the coating layer (Figure 12). At 0.1 A g^{-1} (Figure 13a), the second discharge plateau (~2.1 V) remains similar

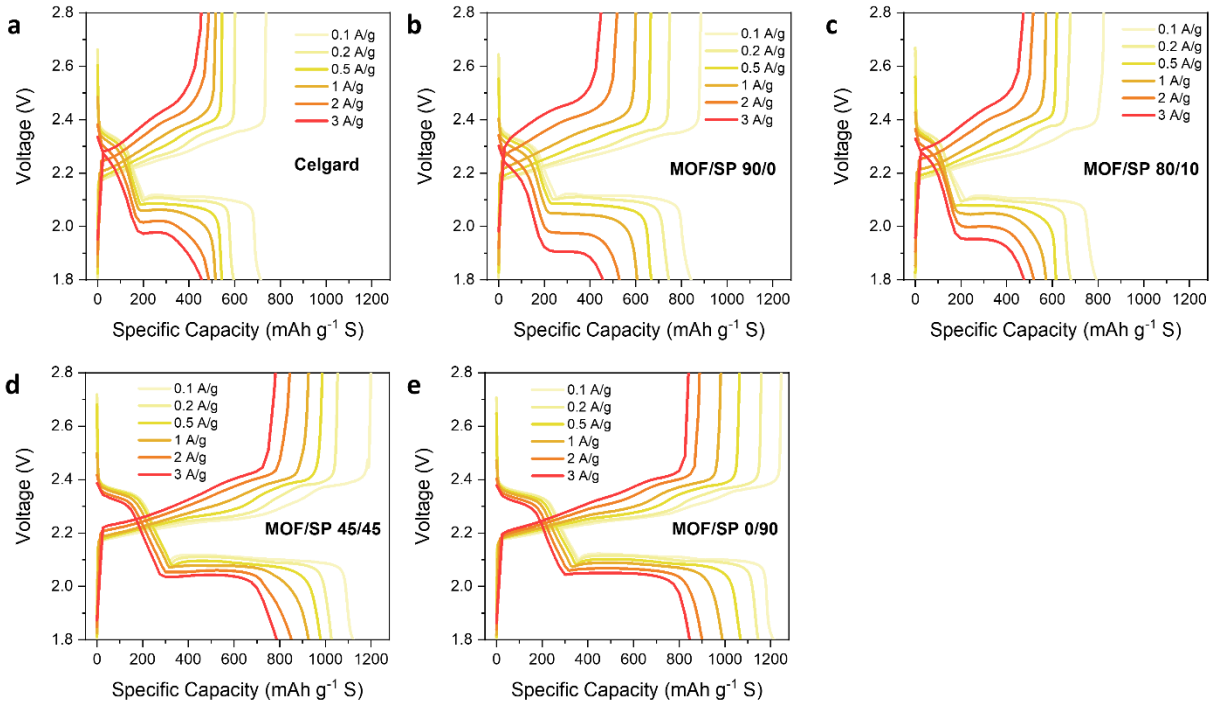

Figure 12. Voltage profiles of Li-S half cells with (a) pristine Celgard membrane and modified Celgard membranes with MOF/SP ratios of: (b) 90/0, (c) 80/10, (d) 45/45 and (e) 0/90.

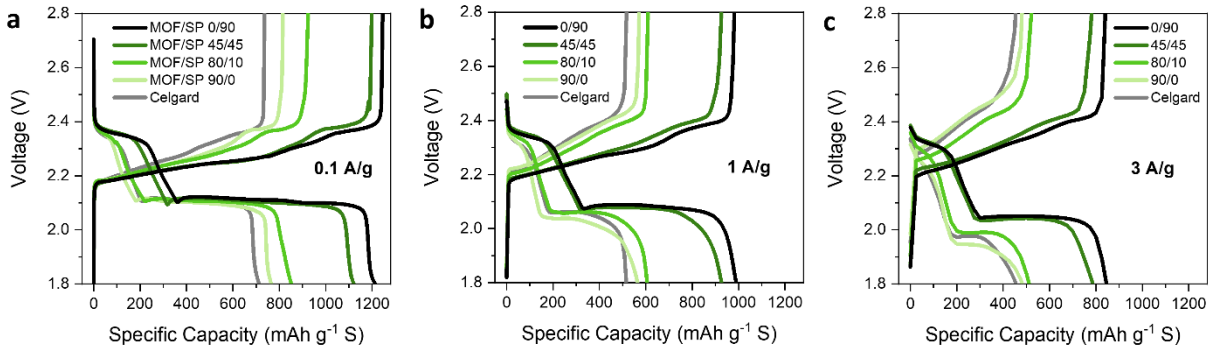

Figure 13. First charge/discharge profiles at: (a) 0.1 A/g, (b) 1 A/g, and (c) 3 A/g.

for all separators and a slight increase in the charge plateau with the decrease in SP content. At a higher rate of 1 A g^{-1} (Figure 13b), the second discharge plateau of the pure MOF modified separator (MOF/SP 90/0) decreased to ~2.05 V, and the charge plateau increased higher. At 3 A g^{-1} (Figure 13c), the increase in overpotential with decrease in SP content is even more obvious in addition to significantly decreased capacity. This trend indicates that not only the initial capacity and capacity retention, but also redox kinetics largely depend on the electrical conductivity of the coating layer.

A CV test was conducted with half cells with the same mass loading at a scan rate of 0.1 mV s^{-1} (Figure 15). In general, two reduction and two oxidation peaks are observed, in which the higher reduction peak (~2.3 V) corresponds to the conversion of S_8 to Li_2S_n ($4 \leq n \leq 8$), and the lower peak (~2.0 V) corresponds to Li_2S_n ($4 \leq n \leq 8$) to Li_2S/Li_2S_2.[37] The reduction peaks show a positive shift, and the oxidation peaks show a negative shift with the increase of the SP content, which indicates the reduction of polarization due to the increased electron pathway available to active sulfur species. Also, the increase in specific current with more SP content indicates the more utilization of sulfur species, and the stable peaks of the modified separators in full CV profiles (Figure 14) show stable cycling of the modified separators. The EIS data of half cells were collected before and after 20 cycles (Figure 16). After 20 cycles, it shows that the electrode charge-

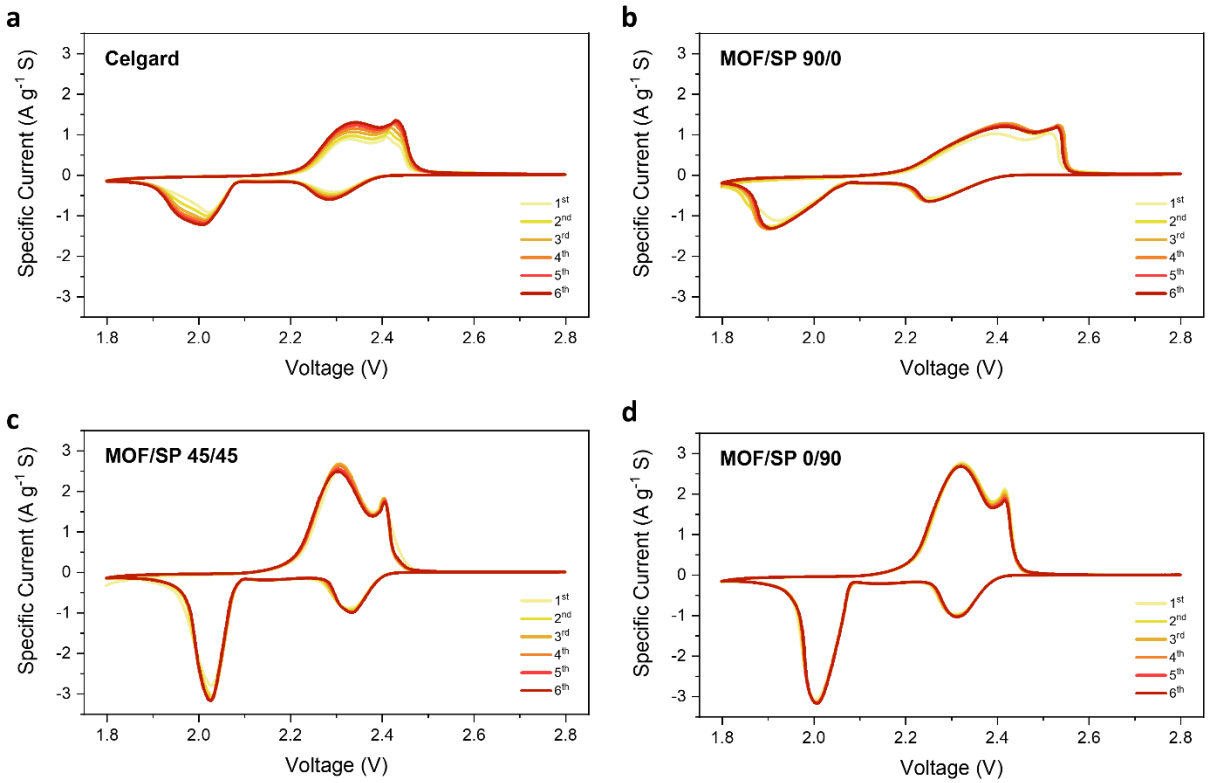

Figure 14. CV profiles of Li-S half cells with (a) pristine Celgard membrane and modified Celgard membranes with MOF/SP ratios of: (b) 90/0, (c) 45/45, and (d) 0/90.

transfer impedance decreased with increased SP content, where MOF/SP 90/0, 80/10, 45/45, and 0/90 have 16, 13, 7, and 4 Ω, respectively. The reduced impedance and increased utilization of sulfur can be ascribed to higher electrical conductivity of the coating layer which facilitates the charge transfer of redox reaction with sulfur species.

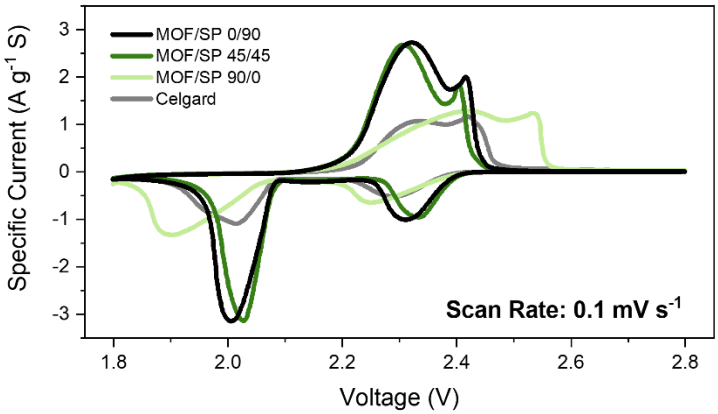

Figure 15. CV profiles of Li-S half cells using MOF/SP modified separators with different MOF to SP ratio.

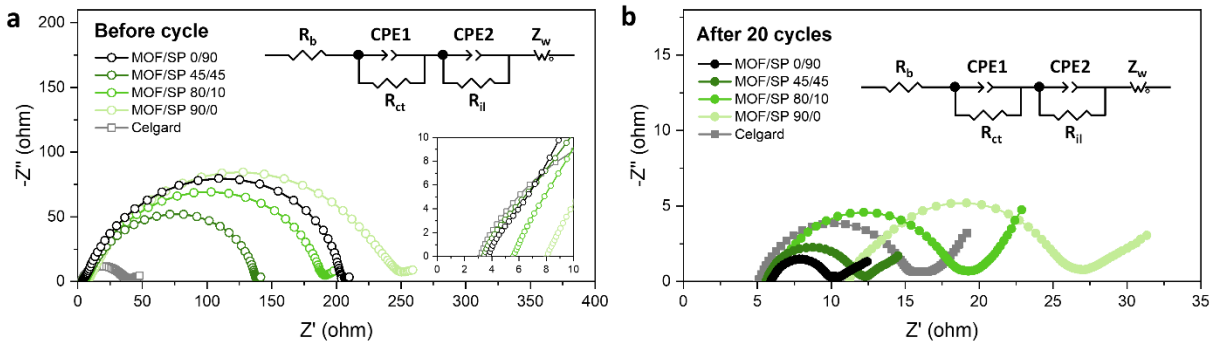

Figure 16. EIS data of Li-S half cells with pristine and modified Celgard membranes (a) before cycling and (b) after 20 cycles with corresponding equivalent circuit.

In order to understand the behavior of the MOF/SP coated separators with increased sulfur content, half cells with high sulfur loading cathodes (3.5 mg cm^{-2}) were assembled by using MOF/SP with 45/45 and 0/90 ratio (Figure 17). The initial capacities were 888, 936, and 446 mAh g^{-1} for cells with MOF/SP 45/45, MOF/SP 0/90, and the pristine Celgard membrane, respectively. The superior performance of the pure SP modified separator can be attributed to the better sulfur utilization in thick cathodes. Because the high sulfur loading cathodes suffer from the low utilization of sulfur due to insufficient electron pathway, the high electrical conductivity of the modified separator dominates the performance. Based on the above results, it would appear that the superior performance of the pure SP modified separator renders MOFs not a critical functional

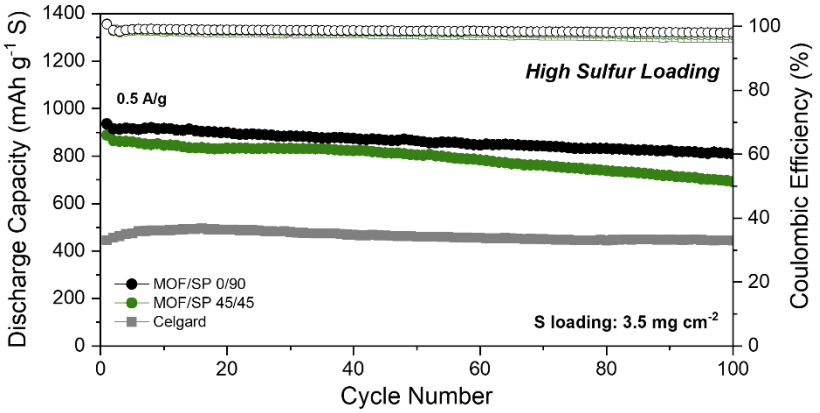

Figure 17. Cycling performance of Li-S half cells with MOF/SP coated separators with high sulfur loading cathode (3.5 mg cm^{-2}).

component. However, a relatively thick coating layer (~40 μm) was deliberately used in our earlier experiments to demonstrate the relation between electrical conductivity and the performance of the modified separators.

3.4 Effect of the thickness and MOF loading of MOF/SP layer

For practical application, it is necessary to have the coating layer as light and thin as possible because additional thickness is dead weight that eventually decreases the gravimetric and volumetric energy densities of batteries.[38] To achieve the highest possible energy density, thinner layers of MOF/SP 45/45 and 0/90 modified separators were prepared, and their thicknesses were verified by cross-sectional SEM images (Figure 18). MOF/SP 45/45 was prepared with coating thicknesses of 25 and 18 μm, while MOF/SP 0/90 was prepared with coating thicknesses of 24 and

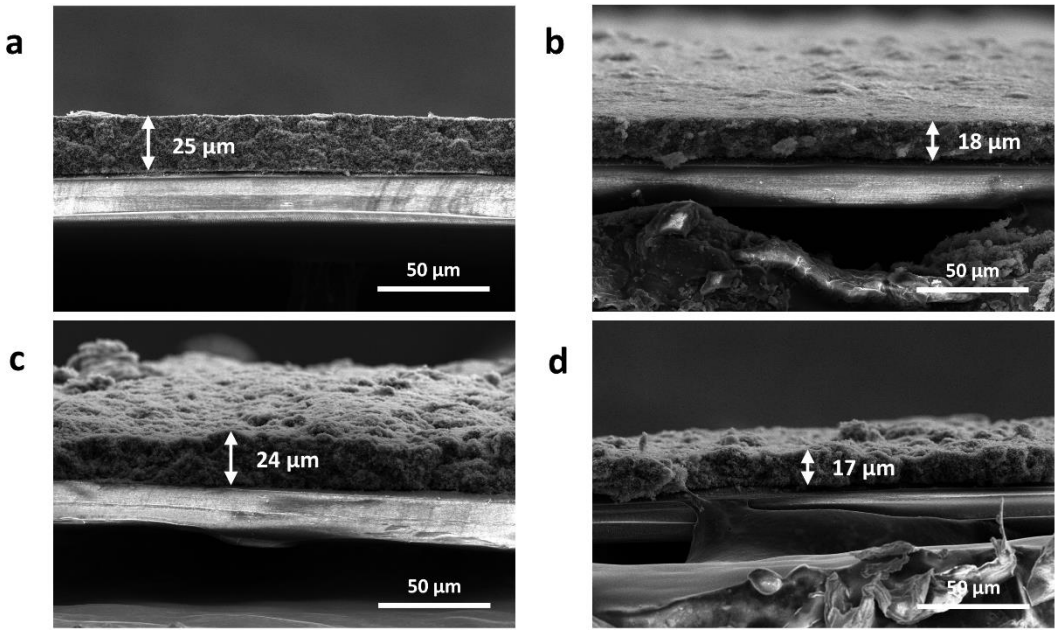

Figure 18. Cross-sectional SEM images of modified Celgard membranes with MOF/SP ratios of 45/45 with thicknesses of: (a) 25 μm and (b) 18 μm and 0/90 with thicknesses of: (c) 24 μm and (d) 17 μm.

17 μm. With such thin modified separators, Li-S half cells were assembled and cycled at 0.5 A g^{-1} (Figure 19a). For MOF/SP 45/45, the average capacities remained similar for the 25 and 18 μm (914 and 907 mAh g^{-1}, respectively) (Figure 19b). By comparison, for MOF/SP 0/90, the average capacity of the cell with 17 μm coating layer was significantly lower than that of 24 μm (813 and 1035 mAh g^{-1}, respectively). This flipped trend between MOF/SP 45/45 and 0/90 can be explained

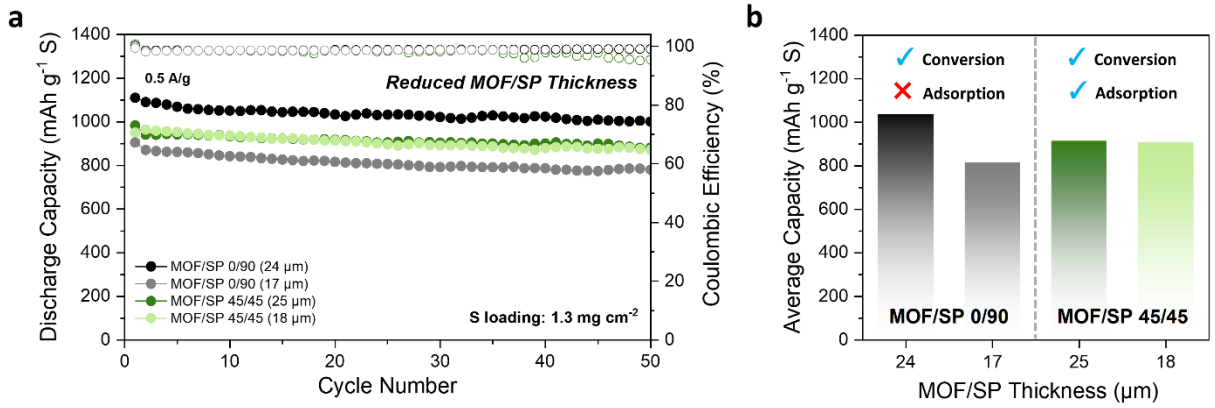

Figure 19. (a) Cycling performance and (b) average discharge capacities of Li-S half cells with MOF/SP coated separators with reduced MOF/SP thickness.

by the synergetic effects of adsorption (attributed to the MOF porous structure) and conversion (associated with the electrical conductivity) of LiPS. For the separators with both LiPS adsorption and conversion capabilities (e.g., MOF/SP 45/45), despite the shorter diffusion length (small membrane thickness), MOFs adsorb LiPS to prevent the loss of LiPS species while the electron pathway of SP enables the re-utilization of the trapped LiPS species. However, for the separators with strong conversion capability but weak adsorption capability (e.g., MOF/SP 0/90), the diffusion length solely determines the degree of LiPS utilization for reaction, thus the decrease in thickness significantly deteriorates the performance.

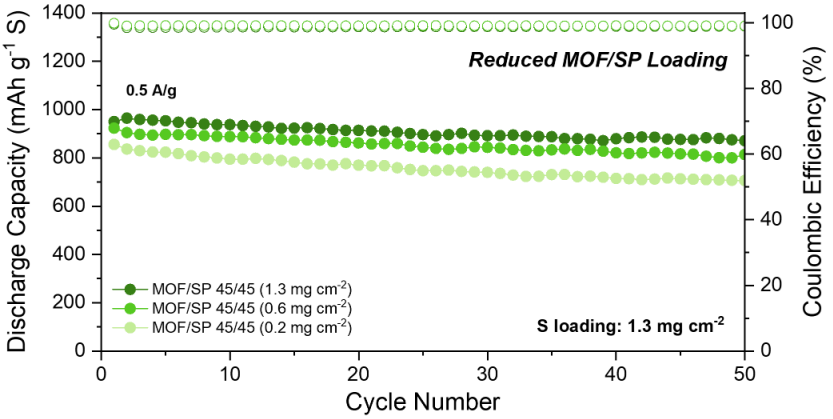

Figure 20. Cycling performance of Li-S half cells with MOF/SP coated separators reduced MOF/SP loading while fixed MOF/SP ratio of 45/45.

After understanding the synergetic effects of adsorption and conversion at limited diffusion length of composite layers, these two counterbalancing capabilities were further investigated by reducing the MOF/SP ratios while fixing the mass loading of the composite layer. Because a noticeable capacity drop was observed for MOF/SP 45/45 at reduced composite loading (below 0.6 mg cm^{-2}) (Figure 20), half cells were assembled using lower MOF ratios with a fixed composite loading of 0.6 mg cm^{-2} (Figure 21a). It was observed that increasing the conversion capability (MOF/SP 45/45 and 30/60) gives higher average capacities (871 and 1008 mAh g^{-1}, respectively), while further increase (MOF/SP 10/80 and 0/90) lowers the capacities (966 and 802 mAh g^{-1},

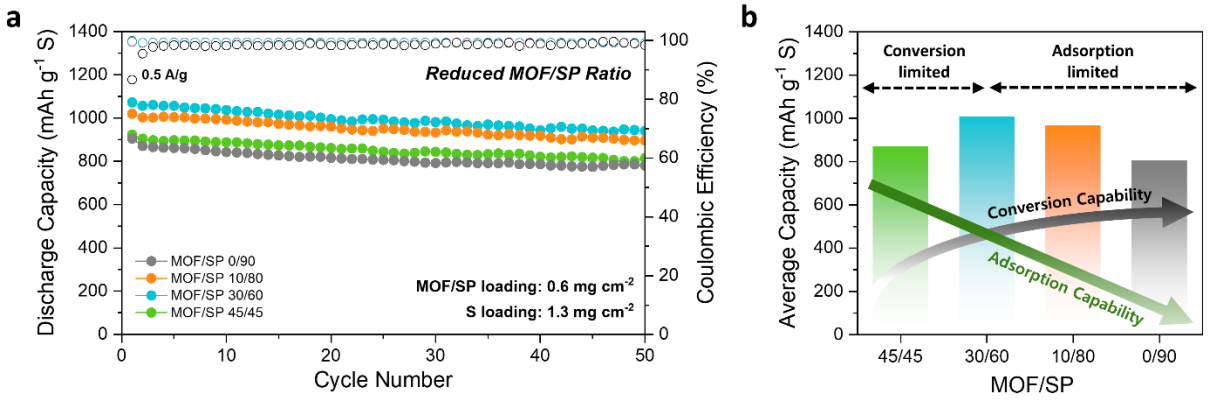

Figure 21. (a) Cycling performance and (b) average discharge capacities of Li-S half cells with MOF/SP coated separators with reduced MOF/SP ratio while fixed MOF/SP loading (0.6 mg cm^{-2}).

respectively) (Figure 21b). This trend indicates that conversion is limited for MOF/SP 45/45 and adsorption is limited for MOF/SP 10/80 and 0/90 based on the highest average discharge capacity for MOF/SP 30/60. This result indicates that an optimal balance between the adsorption and conversion capabilities in a thin composite layer is necessary to achieve both high capacity and stable cycling performance without obviously increasing the inactive components.

CHAPTER 4. CONCLUSION AND FUTURE WORK

4.1 Conclusion

In summary, we show a different perspective of understanding the property-performance relation of MOF/SP modified separators in Li-S batteries by adjusting the MOF/SP ratio, thickness and mass loading of the composite. The electrochemical results show that the modified layers with higher electrical conductivity have significantly improved performance, thereby decreasing the impedance and overpotential at various charge/discharge rates. On the other hand, the LiPS adsorption property becomes crucial when the diffusion length is limited (*i.e.*, reduced composite thickness) and electrical conductivity is saturated (*i.e.*, reduced MOF loading). For future applications, an optimal balance between the adsorption and conversion capabilities of a thin and light composite layer is necessary to achieve the long-life and highest energy density. This work aims to clarify the synergetic effects between the LiPS adsorption property of MOFs and conversion property of conductive materials of the modified separators in Li-S batteries, and thus providing a better understanding on the role of MOFs in such modified separators.

4.2 Future work

This work aims to provide a different perspective of understanding the property-performance relation by means of electrochemical analyses. In order to support the finding of this work, advanced characterizations and computational simulations can be conducted to understand the complex adsorption and conversion kinetics of LiPS species inside MOF/SP composites. The deeper understanding of the complex kinetic can help researchers to build and understand new MOF-based functional separators.

Acknowledgement

This work was supported by the National Science Foundation through the U.C. San Diego Materials Research Science and Engineering Center (UCSD MRSEC). This work was performed in part at the San Diego Nanotechnology Infrastructure (SDNI) of U.C. San Diego. Material characterization was supported by a grant from the Department of Energy, Office of Basic Energy Sciences, Division of Materials Science and Engineering.

This work is currently being prepared for submission for publication: Dong Ju Lee, Xiaolu Yu, R. Eric Sikma, Mingqian Li, Seth M. Cohen, Guorui Cai*, and Zheng Chen*, "Holistic Design Consideration of Metal-Organic Framework-Based Membranes for Lithium-Sulfur Batteries". The thesis author was the primary author of this publication.

REFERENCES

1.Zhao, C.; Xu, G.-L.; Yu, Z.; Zhang, L.; Hwang, I.; Mo, Y.-X.; Ren, Y.; Cheng, L.; Sun, C.-J.; Ren, Y., A high-energy and long-cycling lithium–sulfur pouch cell via a macroporous catalytic cathode with double-end binding sites. Nat. Nanotechnol. 2021, 16 (2), 166-173.

2.Liu, D.; Zhang, C.; Zhou, G.; Lv, W.; Ling, G.; Zhi, L.; Yang, Q. H., Catalytic effects in lithium–sulfur batteries: promoted sulfur transformation and reduced shuttle effect. Adv. Sci. 2018, 5 (1), 1700270.

3.Lim, W. G.; Kim, S.; Jo, C.; Lee, J., A comprehensive review of materials with catalytic effects in Li–S batteries: enhanced redox kinetics. Angew. Chem. Int. Ed. 2019, 58 (52), 18746-18757.

4.Pang, Q.; Liang, X.; Kwok, C. Y.; Nazar, L. F., Advances in lithium–sulfur batteries based on multifunctional cathodes and electrolytes. Nat. Energy 2016, 1, 16132.

5.Safari, M.; Kwok, C.; Nazar, L., Transport properties of polysulfide species in lithium–sulfur battery electrolytes: coupling of experiment and theory. ACS Cent. Sci. 2016, 2 (8), 560-568.

6.Li, G.; Lei, W.; Luo, D.; Deng, Y.; Deng, Z.; Wang, D.; Yu, A.; Chen, Z., Stringed “tube on cube” nanohybrids as compact cathode matrix for high-loading and lean-electrolyte lithium–sulfur batteries. Energy Environ. Sci. 2018, 11 (9), 2372-2381.

7.Li, G.; Wang, S.; Zhang, Y.; Li, M.; Chen, Z.; Lu, J., Revisiting the role of polysulfides in lithium–sulfur batteries. Adv. Mater. 2018, 30 (22), 1705590.

8.Zhang, G.; Peng, H. J.; Zhao, C. Z.; Chen, X.; Zhao, L. D.; Li, P.; Huang, J. Q.; Zhang, Q., The radical pathway based on a lithium-metal-compatible high-dielectric electrolyte for lithium–sulfur batteries. Angew. Chem. Int. Ed. 2018, 57, 16732-16736.

9.Zhong, Y.; Yin, L.; He, P.; Liu, W.; Wu, Z.; Wang, H., Surface chemistry in cobalt phosphide-stabilized lithium–sulfur batteries. J. Am. Chem. Soc. 2018, 140 (4), 1455-1459.

10.Xu, R.; Li, J. C.; Lu, J.; Amine, K.; Belharouak, I., Demonstration of highly efficient lithium–sulfur batteries. J. Mater. Chem. A 2015, 3 (8), 4170-4179.

11.Zhang, J.; Li, Z.; Chen, Y.; Gao, S.; Lou, X. W., Nickel–iron layered double hydroxide hollow polyhedrons as a superior sulfur host for lithium–sulfur batteries. Angew. Chem. Int. Ed. 2018, 57, 10944-10948.

12.Yang, Z.; Peng, C.; Meng, R.; Zu, L.; Feng, Y.; Chen, B.; Mi, Y.; Zhang, C.; Yang, J., Hybrid anatase/rutile nanodots-embedded covalent organic frameworks with complementary polysulfide adsorption for high-performance lithium–sulfur batteries. ACS Cent. Sci. 2019, 5, 1876-1883.

13.Chen, H.; Zhou, G.; Boyle, D.; Wan, J.; Wang, H.; Lin, D.; Mackanic, D.; Zhang, Z.; Kim, S. C.; Lee, H. R., Electrode design with integration of high tortuosity and sulfur-philicity for high-performance lithium-sulfur battery. Matter 2020, 2 (6), 1605-1620.

14.Jin, Z.; Lin, T.; Jia, H.; Liu, B.; Zhang, Q.; Li, L.; Zhang, L.; Su, Z.-m.; Wang, C., Expediting the conversion of Li2S2 to Li2S enables high-performance Li–S batteries. ACS Nano 2021, 15 (4), 7318-7327.

15.Jiang, H.; Liu, X. C.; Wu, Y.; Shu, Y.; Gong, X.; Ke, F. S.; Deng, H., Metal–organic frameworks for high charge–discharge rates in lithium–sulfur batteries. Angew. Chem. Int. Ed. 2018, 57, 3916-3921.

16.Kim, S. H.; Yeon, J. S.; Kim, R.; Choi, K. M.; Park, H. S., A functional separator coated with sulfonated metal–organic framework/Nafion hybrids for Li–S batteries. J. Mater. Chem. A 2018, 6 (48), 24971-24978.

17.Han, D.-D.; Wang, Z.-Y.; Pan, G.-L.; Gao, X.-P., Metal–organic-framework-based gel polymer electrolyte with immobilized anions to stabilize a lithium anode for a quasi-solid-state lithium–sulfur battery. ACS Appl. Mater. Interfaces 2019, 11 (20), 18427-18435.

18.Tian, M.; Pei, F.; Yao, M.; Fu, Z.; Lin, L.; Wu, G.; Xu, G.; Kitagawa, H.; Fang, X., Ultrathin MOF nanosheet assembled highly oriented microporous membrane as an interlayer for lithium-sulfur batteries. Energy Storage Mater. 2019, 21, 14-21.

19.Cai, G.; Yan, P.; Zhang, L.; Zhou, H.-C.; Jiang, H.-L., Metal–organic framework-based hierarchically porous materials: Synthesis and applications. Chem. Rev. 2021, 121, 12278–12326.

20.Cai, G.; Yin, Y.; Xia, D.; Chen, A. A.; Holoubek, J.; Scharf, J.; Yang, Y.; Koh, K. H.; Li, M.; Davies, D. M.; Mayer, M.; Han, T. H.; Meng, S. Y.; Pascal, T. A.; Chen, Z., Sub-nanometer confinement enables facile condensation of gas electrolyte for low-temperature batteries. Nat. Commun. 2021, 12, 3395.

21.Han, J.; Gao, S.; Wang, R.; Wang, K.; Jiang, M.; Yan, J.; Jin, Q.; Jiang, K., Investigation of the mechanism of metal–organic frameworks preventing polysulfide shuttling from the perspective of composition and structure. J. Mater. Chem. A 2020, 8 (14), 6661-6669.

22.Qi, C.; Xu, L.; Wang, J.; Li, H.; Zhao, C.; Wang, L.; Liu, T., Titanium-containing metal–organic framework modified separator for advanced lithium–sulfur batteries. ACS Sustain. Chem. Eng. 2020, 8 (34), 12968-12975.

23.Bai, S.; Liu, X.; Zhu, K.; Wu, S.; Zhou, H., Metal–organic framework-based separator for lithium–sulfur batteries. Nat. Energy 2016, 1, 16094.

24.Yuan, N.; Sun, W.; Yang, J.; Gong, X.; Liu, R., Multifunctional MOF-based separator materials for advanced lithium–sulfur batteries. Adv. Mater. Interfaces 2021, 8 (9), 2001941.

25.Zhu, D.; Long, T.; Xu, B.; Zhao, Y.; Hong, H.; Liu, R.; Meng, F.; Liu, J., Recent advances in interlayer and separator engineering for lithium-sulfur batteries. J. Energy Chem. 2021, 57, 41-60.

26.He, Y.; Chang, Z.; Wu, S.; Qiao, Y.; Bai, S.; Jiang, K.; He, P.; Zhou, H., Simultaneously inhibiting lithium dendrites growth and polysulfides shuttle by a flexible MOF-based membrane in Li–S batteries. Adv. Energy Mater. 2018, 8 (34), 1802130.

27.Lee, D. H.; Ahn, J. H.; Park, M.-S.; Eftekhari, A.; Kim, D.-W., Metal-organic framework/carbon nanotube-coated polyethylene separator for improving the cycling performance of lithium-sulfur cells. Electrochim. Acta 2018, 283, 1291-1299.

28.Fan, Y.; Niu, Z.; Zhang, F.; Zhang, R.; Zhao, Y.; Lu, G., Suppressing the shuttle effect in lithium–sulfur batteries by a UiO-66-modified polypropylene separator. ACS Omega 2019, 4 (6), 10328-10335.

29.Wang, X.; Zhao, Y.; Wu, F.; Liu, S.; Zhang, Z.; Tan, Z.; Du, X.; Li, J., ZIF-7@carbon composites as multifunctional interlayer for rapid and durable Li-S performance. J. Energy Chem. 2021, 57, 19-27.

30.Zheng, S.; Zhao, X.; Liu, G.; Wu, F.; Li, J., A multifunctional UiO-66@carbon interlayer as an efficacious suppressor of polysulfide shuttling for lithium-sulfur batteries. Nanotechnology 2021, 32, 365404.

31.Guo, S.; Xiao, Y.; Wang, J.; Ouyang, Y.; Li, X.; Deng, H.; He, W.; Zeng, Q.; Zhang, W.; Zhang, Q., Ordered structure of interlayer constructed with metal-organic frameworks improves the performance of lithium-sulfur batteries. Nano Research 2021, 14, 4556–456.

32.Cai, G.; Ma, X.; Kassymova, M.; Sun, K.; Ding, M.; Jiang, H.-L., Large-scale production of hierarchically porous metal–organic frameworks by a reflux-assisted post-synthetic ligand substitution strategy. ACS Cent. Sci. 2021, 7 (8), 1434-1440.

33.Guo, S.; Xiao, Y.; Wang, J.; Ouyang, Y.; Li, X.; Deng, H.; He, W.; Zeng, Q.; Zhang, W.; Zhang, Q., Ordered structure of interlayer constructed with metal-organic frameworks improves the performance of lithium-sulfur batteries. Nano Research 2021, 14, 4556–4562.

34.Li, S.; Lin, J.; Ding, Y.; Xu, P.; Guo, X.; Xiong, W.; Wu, D.-Y.; Dong, Q.; Chen, J.; Zhang, L., Defects engineering of lightweight metal–organic frameworks-based electrocatalytic membrane for high-loading lithium–sulfur batteries. ACS Nano 2021, 15 (8), 13803-13813.

35.Suriyakumar, S.; Stephan, A. M.; Angulakshmi, N.; Hassan, M. H.; Alkordi, M. H., Metal–organic framework@SiO2 as permselective separator for lithium–sulfur batteries. J. Mater. Chem. A 2018, 6 (30), 14623-14632.

36.Brückner, J.; Thieme, S.; Grossmann, H. T.; Dörfler, S.; Althues, H.; Kaskel, S., Lithium–sulfur batteries: Influence of C-rate, amount of electrolyte and sulfur loading on cycle performance. J. Power Sources 2014, 268, 82-87.

37.Hong, X.-J.; Song, C.-L.; Yang, Y.; Tan, H.-C.; Li, G.-H.; Cai, Y.-P.; Wang, H., Cerium based metal–organic frameworks as an efficient separator coating catalyzing the conversion of polysulfides for high performance lithium–sulfur batteries. ACS Nano 2019, 13 (2), 1923-1931.

38.Chung, S. H.; Chang, C. H.; Manthiram, A., Progress on the critical parameters for lithium–sulfur batteries to be practically viable. Adv. Funct. Mater. 2018, 28 (28), 1801188.